Proceedings of the ASME 2018
Dynamic Systems and Control Conference
DSCC2018
September 30-October 3, 2018, Atlanta, Georgia, USA

DSCC2018-9200

DISTURBANCE OBSERVER-BASED MOTION CONTROL OF SMALL AUTONOMOUS UNDERWATER VEHICLES

Bingheng Wang
School of Astronautics
Northwestern Polytechnical University
Xi'an, Shannxi, 710072, P. R. China
Email: bingheng_wang@mail.nwpu.edu.cn

Marko Mihalec[1], Yongbin Gong[1], Dario Pompili[2], Jingang Yi[1]*
[1]Dept. of Mech. Aero. Eng., [2]Dept. of Elec. Comp. Eng.
Rutgers, The State University of New Jersey
Piscataway, New Jersey 08854
Email: {yongbin.gong,marko.mihalec,pompili,jgyi}@.rutgers.edu

ABSTRACT

This paper presents a trajectory-tracking method using disturbance observer-based model predictive control (MPC) for small autonomous underwater vehicles (AUV). The goal of the work is to design a robust motion controller for AUVs under the system constraints and unknown disturbances such as hydrodynamics and ocean currents. Super-twisting-algorithm (STA) is employed to design the disturbance observer and its output is used and included in the feedback linearization law to compensate for the disturbances. The control inputs are generated using the MPC design with the nominal linearized model. Simulation results are included to validate the effectiveness of the control design and also compare with the traditional MPC motion control.

NOMENCLATURE

x, y, z	An earth-fixed frame coordinate system.
x_b, y_b, z_b	A body-fixed frame coordinate system.
ϕ, θ, ψ	Roll, Pitch, Yaw angle in earth-fixed frame.
$\boldsymbol{v}_c$	Velocity vector of irrotational current in earth-fixed frame.
$\boldsymbol{v}^b$	Velocity vector of AUV in body-fixed frame.
$\boldsymbol{v}_r^b$	Relative velocity vector of AUV in body-fixed frame.
$\boldsymbol{v}_h^b$	Horizontal velocity vector of AUV in body-fixed frame.
$\boldsymbol{v}_{hc}^b$	Unknown current horizontal velocity vector in body-fixed frame.
$\boldsymbol{\eta}$	Pose of AUV in earth-fixed frame.
$\boldsymbol{\eta}_h$	Horizontal pose of AUV in earth-fixed frame.
$\boldsymbol{\tau}_e^b$	Environment forces and moments expressed in body-fixed frame.
$\boldsymbol{\tau}_F^b$	Thrust forces and moments expressed in body-fixed frame.
$\boldsymbol{\tau}_{hF}^b$	Thrust forces and moments in horizontal plane expressed in body-fixed frame.
$\boldsymbol{d}$	Lumped disturbances related to unknown hydrodynamics and currents.
$\boldsymbol{d}_m$	Unknown disturbances which are estimated by STA-based observer.
$\boldsymbol{z}$	Observer internal state.
$\boldsymbol{F}_h$	Thrust force acting on the system.
$\boldsymbol{F}_{hmin}$	Minimum thrust force system can provide.
$\boldsymbol{F}_{hmax}$	Maximum thrust force system can provide.
$\boldsymbol{F}_{mpc}$	MPC controller output.
$\boldsymbol{e}$	Tracking error.
$\boldsymbol{C}_g$	Center of geometry of AUV.
$\boldsymbol{C}_m$	Center of mass of AUV.
$\boldsymbol{C}_B$	Center of buoyancy of AUV.

INTRODUCTION

Trajectory tracking plays a vital role in the wide applications of small autonomous underwater vehicles (AUVs) that are used in ocean, river, and lake explorations. Motion control of

*Address all correspondence to this author.

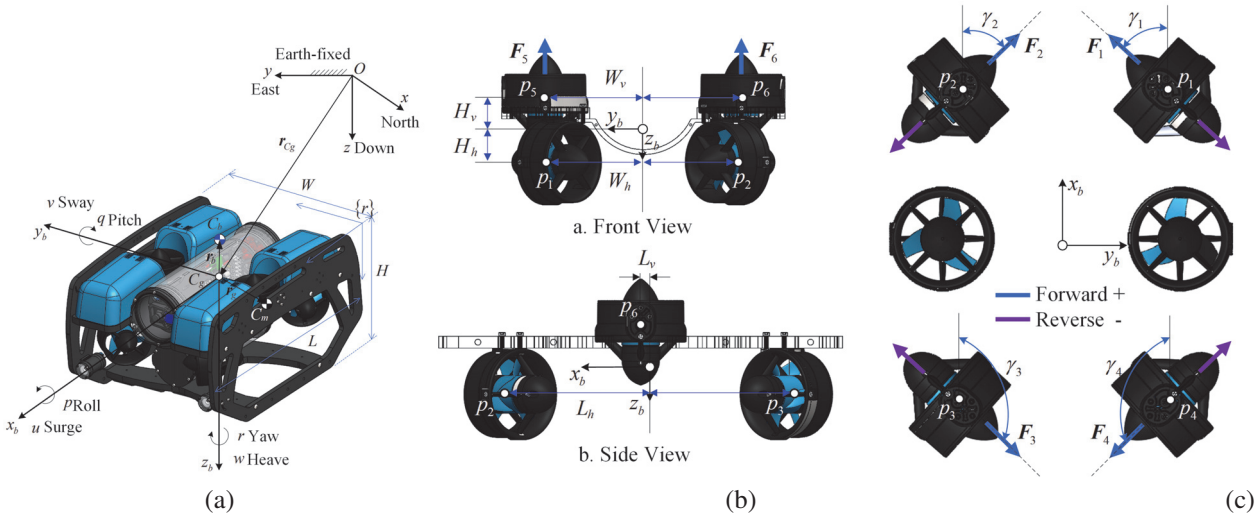

Figure 1. (a) An overview structure and coordinate frames of the BLUEROV2. (b) and (c) for thruster orientations and frames.

small AUVs is nontrivial due two main challenges: (1) System model uncertainties, such as added mass and hydrodynamic effects. These uncertainties complicate the modeling approaches and degrade the model accuracy [1]; and (2) unknown underwater conditions, such as the disturbances of water currents and the interactions with waves. To overcome the above-mentioned challenges, a robust controller is needed for small AUVs. The goal of this paper is to develop a robust motion control for small AUVs under model uncertainty and external disturbances.

Sliding mode control (SMC) has obtained much attention [2] and shown effectiveness for controlling AUVs under the presence of disturbances and uncertainties. Gomes et al. [3] used a PID-based multivariable SMC to contorl an AUV to follow the trajectory while resisting the uncertainty. Dyda et al. [4] aimed to improve the characteristic of a remotely operated underwater vehicles (ROV) system by designing a novel switching sliding surface. Zhang and Chu [5] employed a neural network model to estimate the AUV estimates and then designed an adaptive SMC scheme to mitigate the chattering effect. There are also lots of efforts dedicated to the mitigation of the SMC chattering effect for underwater vehicle [6, 7]. In [8, 9], the robustness of SMC was further enhanced by an adaptive fuzzy algorithm for underwater disturbance compensation. It is noted that these SMC controllers require the vehicle model to be as accurate as possible, which may not be available in most cases. For this reason, model-free SMC has been proposed and applied to AUVs without any knowledge of the system model [10–12].

Despite the merits of SMC, the main deficiency is that the system constraints, such as thruster limitations and position constraints, cannot be directly taken into account in SMC design. This motivates the application of model predictive control (MPC) to vehicle trajectory-tracking problem [13–15]. Molero et al. [13] demonstrated the better tracking performance using linear MPC with less control effort, comparing with a classical feedback controller. To handle the nonlinearity, Shen et al. [14] used a nonlinear MPC and proposed distributed implementation to alleviate the computational burden of nonlinear programming. However, both of these control designs are based on the condition where the accurate vehicle model can be obtained.

Given the aforementioned modeling challenges and the system constraints, the main contribution of this paper is to propose a robust AUV trajectory-tracking method using a disturbance observer-based model predictive control (DOBMPC) design. We apply the design to a small AUV, called BlueROV2. The model with the specified thrust configuration of BlueROV2 consists of an accurate rigid-body dynamics and a lumped unknown disturbance representing hydrodynamics and water currents. To reduce the computational complexity, a feedback linearization (FBL) law is designed to cancel the nonlinearity, which incorporates an output of super-twisting-algorithm (STA) observer to counteract the disturbances. The control inputs are generated using an MPC design with the nominal linearized model. The MPC-based input is then applied to the actual system by the FBL-based thrust mapping.

The rest of this paper is organized as follows. The BlueROV2 model is first presented along with the simplification in horizontal motion. The detailed development of DOBMPC is then proposed. Finally, simulation results are presented to show the tracking control performance and also comparing with the traditional MPC method.

THE BLUEROV2 MODEL

As a high-performance underwater vehicle, BlueROV2 features high maneuverability and rugged reliability and has been

proven successful in ocean-related research and inspection. The weight of the vehicle is around 10 kg (without ballast) and with ballast is around 11 kg. The vehicle has a small size (457mm $\times$ 338 $\times$ 254 mm) and can dive for maximum 100 m. There are six thrusters on the vehicle: four vectored and two vertical. The main onboard sensors include inertial measurement units (IMU) with magnetometer, a camera, a depth sensor and other sensors such as water pH value and salinity, etc.

Two coordinate frames are setup for modeling. An earth-fixed frame is defined as an inertial frame $\{i\}$ with x axis pointing towards north, y axis pointing towards east and z pointing downwards. A body-fixed frame $\{b\}$ is defined with the origin C_g fixed in the center of geometry and three axes pointing towards longitudinal, lateral and normal directions, respectively as shown in Fig. **??**, where C_g can be located using the coordinate $\frac{1}{2}[L,W,H]^T$ based on the corner frame $\{r\}$. Compared with fixing the body frame at the mass center C_m or the buoyancy center C_b, the body frame fixed in C_g has two benefits: (1) C_m may move depending on the actual load condition and (2) using C_g can take advantages of the robot geometrical properties, such as symmetry. By [16, 17], the equations of motion for the vehicle are obtained as

$$\boldsymbol{M}\dot{\boldsymbol{\nu}}_r^b + \boldsymbol{C}\left(\boldsymbol{\nu}_r^b\right)\boldsymbol{\nu}_r^b + \boldsymbol{D}\left(\boldsymbol{\nu}_r^b\right)\boldsymbol{\nu}_r^b + \boldsymbol{g}\left(\boldsymbol{\eta}\right) = \boldsymbol{\tau}_e^b + \boldsymbol{\tau}_F^b \tag{1}$$

$$\underbrace{\begin{bmatrix}\dot{\boldsymbol{\eta}}_1\\ \dot{\boldsymbol{\eta}}_2\end{bmatrix}}_{\boldsymbol{\eta}} = \underbrace{\begin{bmatrix}\boldsymbol{J}_1\left(\boldsymbol{\eta}_1\right)\boldsymbol{0}_{3\times3}\\ \boldsymbol{0}_{3\times3}\boldsymbol{J}_2\left(\boldsymbol{\eta}_2\right)\end{bmatrix}}_{\boldsymbol{J}(\boldsymbol{\eta})}\underbrace{\begin{bmatrix}\boldsymbol{\nu}_{1r}^b\\ \boldsymbol{\nu}_{2r}^b\end{bmatrix}}_{\boldsymbol{\nu}_r^b} + \boldsymbol{\nu}_c \tag{2}$$

where $\boldsymbol{\eta}_1 = [xyz]^T$ and $\boldsymbol{\eta}_2 = [\phi\,\theta\,\psi]^T$ are positions and orientation vectors in $\{i\}$, respectively, $\boldsymbol{\nu}_r^b = \boldsymbol{\nu}^b - \boldsymbol{J}_1^{-1}\left(\boldsymbol{\eta}_2\right)\boldsymbol{\nu}_c$ is the relative velocity, $\boldsymbol{\nu}^b = [u,v,w,p,q,r]^T$ is the AUV absolute velocity in $\{b\}$ and $\boldsymbol{\nu}_c = [u_c,v_c,w_c,0,0,0]^T$ is the irrotational current velocity in $\{i\}$. $\boldsymbol{M} = \boldsymbol{M}_{RB} + \boldsymbol{M}_A$, $\boldsymbol{M}_{RB}$ is the inertia matrix and $\boldsymbol{M}_A$ is the added mass matrix. $\boldsymbol{C}\left(\boldsymbol{\nu}_r^b\right) = \boldsymbol{C}\left(\boldsymbol{\nu}_r^b\right)_{RB} + \boldsymbol{C}_A\left(\boldsymbol{\nu}_r^b\right)$ is the Coriolis and centripetal matrix due to inertia and hydrodynamics, $\boldsymbol{D}\left(\boldsymbol{\nu}_r^b\right)$ is the hydrodynamic damping matrix, $\boldsymbol{g}\left(\boldsymbol{\eta}\right)$ is the hydrostatic force and moment, $\boldsymbol{\tau}_e^b$ is the environment force and moment and $\boldsymbol{\tau}_F^b$ represents the thruster forces and moments in $\{b\}$. Since the BlueROV is operating stably in the roll and pitch directions due to a distance between C_m and C_b, Euler angles are sufficient to describe the attitude as in the above equations.

In many cases, it is convenient to develop a planar motion dynamics for control design. To capture the horizontal motion, the simplified model can be obtained by neglecting dynamics associated with the motions in heave, roll and pitch. It is feasible to assume that the equations associated with inertial parameters are known exactly by measurements while all terms regarding ocean current velocities and hydrodynamics are uncertain or even unknown. To this end, the horizontal model takes the following form.

$$\dot{\boldsymbol{\eta}}_h = \boldsymbol{J}_h\left(\boldsymbol{\eta}_h\right)\boldsymbol{\nu}_h^b \tag{3}$$

$$\boldsymbol{M}_{hRB}\dot{\boldsymbol{\nu}}_h^b + \boldsymbol{C}_{hRB}\left(\boldsymbol{\nu}_h^b\right)\boldsymbol{\nu}_h^b = \boldsymbol{\tau}_{hF}^b + \boldsymbol{d}, \tag{4}$$

where $\boldsymbol{\eta}_h = [x\,y\,\psi]^T$ and $\boldsymbol{\nu}_h^b = [u\,v\,r]^T$ are horizontal positions in $\{i\}$ and velocities in $\{b\}$, respectively, $\boldsymbol{J}_h\left(\boldsymbol{\eta}_h\right) \in \mathbb{R}^{3\times3}$ is the horizontal Jacobian matrix, $\boldsymbol{M}_{hRB} \in \mathbb{R}^{3\times3}$ and $\boldsymbol{C}_{hRB}\left(\boldsymbol{\nu}_h^b\right) \in \mathbb{R}^{3\times3}$ are the measurable inertial and non-inertial matrices, while $\boldsymbol{d} = \boldsymbol{M}_{hRB}\dot{\boldsymbol{\nu}}_{hc}^b - \boldsymbol{M}_{hA}\dot{\boldsymbol{\nu}}_{hr}^b + \boldsymbol{C}_{hRB}\left(\boldsymbol{\nu}_h^b\right)\boldsymbol{\nu}_{hc}^b + \boldsymbol{C}_{hRB}\left(\boldsymbol{\nu}_{hc}^b\right)\boldsymbol{\nu}_{hr}^b - \boldsymbol{C}_{hA}\left(\boldsymbol{\nu}_{hr}^b\right)\boldsymbol{\nu}_{hr}^b - \boldsymbol{D}_h\left(\boldsymbol{\nu}_{hr}^b\right)\boldsymbol{\nu}_{hr}^b \in \mathbb{R}^{3\times1}$ is the lumped disturbances related to unknown hydrodynamics and currents. Here, $\boldsymbol{\nu}_{hr}^b = \boldsymbol{\nu}_h^b - \boldsymbol{\nu}_{hc}^b$ is the horizontal relative velocity in $\{b\}$.

The water current magnitude cannot be infinite. For this reason, there exists a positive constant upper boundary $\bar{d}$ such that the disturbances satisfy

$$\|\boldsymbol{d}\|_\infty \leq \bar{d}. \tag{5}$$

The force and torque matrix in horizontal motion satisfies $\boldsymbol{\tau}_{hF}^b = \boldsymbol{B}_h\boldsymbol{F}_h$. Due to symmetry, the vertical thrusters do not affect the horizontal motion and therefore, only four vectored thrusters are taken into account. Matrix $\boldsymbol{B}_h \in \mathbb{R}^{3\times4}$ can be determined by the dimension and the configuration shown in Fig. 1(b) and 1(c). To implement trajectory-tracking, it is advantageous to express (3) as

$$\ddot{\boldsymbol{\eta}}_h = -\boldsymbol{M}_\eta^{-1}\boldsymbol{C}_\eta\dot{\boldsymbol{\eta}}_h + \boldsymbol{M}_\eta^{-1}\boldsymbol{B}_\eta\boldsymbol{F}_h + \boldsymbol{d}_M, \tag{6}$$

where

$$\boldsymbol{M}_\eta = \boldsymbol{J}_h\boldsymbol{M}_{hRB}\boldsymbol{J}_h^{-1} = \begin{bmatrix} m & 0 & -m\left(y_g\mathrm{c}\psi + x_g\mathrm{s}\psi\right)\\ 0 & m & m\left(x_g\mathrm{c}\psi - y_g\mathrm{s}\psi\right)\\ -m\left(y_g\mathrm{c}\psi + x_g\mathrm{s}\psi\right) & m\left(x_g\mathrm{c}\psi - y_g\mathrm{s}\psi\right) & I_z\end{bmatrix},$$

$$\boldsymbol{C}_\eta = \boldsymbol{J}_h\boldsymbol{C}_{hRB}\left(\boldsymbol{\nu}_h^b\right)\boldsymbol{J}_h^{-1} - \boldsymbol{J}_h\boldsymbol{M}_{hRB}\boldsymbol{J}_h^{-1}\dot{\boldsymbol{J}}_h\boldsymbol{J}_h^{-1} = \begin{bmatrix} 0 & mr & -m\mathrm{c}\psi\left(v + rx_g\right) - m\mathrm{s}\psi\left(u - ry_g\right)\\ -mr & 0 & m\mathrm{c}\psi\left(u - ry_g\right) - m\mathrm{s}\psi\left(v + rx_g\right)\\ m\left(v\mathrm{c}\psi + u\mathrm{s}\psi\right) & -m\left(u\mathrm{c}\psi - v\mathrm{s}\psi\right) & 0\end{bmatrix},$$

$$\boldsymbol{B}_\eta = \boldsymbol{J}_h\boldsymbol{B}_h = \begin{bmatrix} \mathrm{c}\left(\gamma_1 + \psi\right) & \mathrm{c}\gamma_2\mathrm{c}\psi - s\gamma_1\mathrm{s}\psi & \mathrm{c}\gamma_3\mathrm{c}\psi - s\gamma_1\mathrm{s}\psi & \mathrm{c}\gamma_4\mathrm{c}\psi - s\gamma_1\mathrm{s}\psi\\ \mathrm{s}\left(\gamma_1 + \psi\right) & \mathrm{c}\psi s\gamma_1 + \mathrm{c}\gamma_2\mathrm{s}\psi & \mathrm{c}\psi s\gamma_1 + \mathrm{c}\gamma_3\mathrm{s}\psi & \mathrm{c}\psi s\gamma_1 + \mathrm{c}\gamma_4\mathrm{s}\psi\\ L_h\mathrm{s}\gamma_1 - W_h\mathrm{c}\gamma_1 & W_h\mathrm{c}\gamma_2 + L_h\mathrm{s}\gamma_2 & W_h\mathrm{c}\gamma_3 - L_h\mathrm{s}\gamma_3 & -W_h\mathrm{c}\gamma_4 - L_h\mathrm{s}\gamma_4\end{bmatrix},$$

and $\boldsymbol{d}_M = \boldsymbol{M}_\eta^{-1}\boldsymbol{J}_h\boldsymbol{d}$. $\mathrm{c}(\cdot)$ and $\mathrm{s}(\cdot)$ represent $\cos(\cdot)$ and $\sin(\cdot)$, respectively.

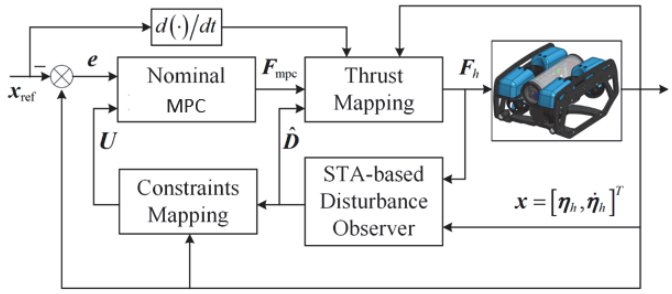

Figure 2. The controller architecture.

DOBMPC DESIGN

The DOBMPC controller consists of a disturbance observer using super-twisting-algorithm (STA) and a feedback linearization (FBL) based model predictive controller. As shown in Fig. 2, optimal control signal $\boldsymbol{F}_{\mathrm{mpc}}$ is generated by a nominal MPC and then applied to the actual perturbed system by a FBL-based thrust mapping. The observer output $\hat{\boldsymbol{D}}$ is added to compensate the disturbances. We do not consider the navigation error and the full states are assumed to be accessible.

STA-based Observer

STA is capable of finite-time convergence and high robustness to uncertainty. Therefore, inspired by [18], a STA-based observer is employed to estimate the unknown disturbances $\boldsymbol{d}_M$. The auxiliary variable used in the observer is defined as $\boldsymbol{\xi}=\boldsymbol{z}-\dot{\boldsymbol{\eta}}_h$, $\boldsymbol{z}\in\mathbb{R}^{3\times1}$ is the observer internal state that satisfies the following dynamic equation.

$$\dot{\boldsymbol{z}} = -\boldsymbol{M}_\eta^{-1}\boldsymbol{C}_\eta\dot{\boldsymbol{\eta}}_h + \boldsymbol{M}_\eta^{-1}\boldsymbol{B}_\eta\boldsymbol{F}_h + \hat{\boldsymbol{D}}, \tag{7}$$

where the STA-based disturbances estimation $\hat{\boldsymbol{D}}$ is designed as

$$\hat{\boldsymbol{D}} = -\boldsymbol{K}_1\sqrt{|\boldsymbol{\xi}|}\mathrm{sign}(\boldsymbol{\xi}) - \int \boldsymbol{K}_2\mathrm{sign}(\boldsymbol{\xi}) \tag{8}$$

where $\boldsymbol{K}_1 = \mathrm{diag}(k_{1i})$ and $\boldsymbol{K}_2 = \mathrm{diag}(k_{2i})$, $i=1,2,3$, are positive definite diagonal gain matrices.

Differentiating $\boldsymbol{xi}$ with the estimation law (7) yields the closed-loop system.

$$\begin{cases} \dot{\boldsymbol{\xi}} = -\boldsymbol{K}_1\sqrt{|\boldsymbol{\xi}|}\mathrm{sign}(\boldsymbol{\xi}) + \boldsymbol{z}_2 - \boldsymbol{d}_M \\ \dot{\boldsymbol{z}}_2 = -\boldsymbol{K}_2\mathrm{sign}(\boldsymbol{\xi}) \end{cases} \tag{9}$$

Theorem 1. *Assuming the each component of $\boldsymbol{d}_M$ is bounded, namely, there is a known positive constant δ_i, such as $|d_{Mi}| \le \delta_i\sqrt{|\xi_i|}$. Therefore, if the parameters in gain matrices satisfy the following condition,*

$$\begin{cases} k_{1i} > 2\delta_i \\ k_{2i} > k_{1i}\dfrac{5\delta_i k_{1i} + 4\delta_i^2}{2(k_{1i}-2\delta_i)} \end{cases} \tag{10}$$

the observer variable $\boldsymbol{\xi}$ and its derivative $\dot{\boldsymbol{\xi}}$ converge to zeros within finite time [19], which guarantees the asymptotical stability of the observer and the accurate estimation of the unknown disturbances.

FBL-based MPC Controller

The FBL law is used to transfer the system (6) to the linear one in order to reduce the computational burden. Replacing $\boldsymbol{d}_M$ with $\hat{\boldsymbol{D}}$, we can obtain the FBL-based thrust mapping that converts the MPC output $\boldsymbol{F}_{\mathrm{mpc}}$ to the thrusts $\boldsymbol{F}_h$ acting on the actual system.

$$\boldsymbol{F}_h = \boldsymbol{B}_\eta^{+}\boldsymbol{C}_\eta\dot{\boldsymbol{\eta}}_h + \boldsymbol{B}_\eta^{+}\boldsymbol{M}_\eta\left(\ddot{\boldsymbol{\eta}}_{\mathrm{ref}} - \hat{\boldsymbol{D}}\right) + \boldsymbol{F}_{\mathrm{mpc}}, \tag{11}$$

where $\boldsymbol{B}_\eta^{+} \in \mathbb{C}_3^{3\times4}$ is the Moore-Penrose inverse of $\boldsymbol{B}_\eta$ and $\ddot{\boldsymbol{\eta}}_{\mathrm{ref}}$ is the reference acceleration. Substituting the FBL law (11) into (6) yields the linear-like system.

$$\ddot{\boldsymbol{\eta}}_h = \boldsymbol{M}_\eta^{-1}\boldsymbol{B}_\eta\boldsymbol{F}_{\mathrm{mpc}} + \ddot{\boldsymbol{\eta}}_{\mathrm{ref}} - \dot{\boldsymbol{\xi}}. \tag{12}$$

With the tracking error $\boldsymbol{e} = \boldsymbol{\eta}_h - \boldsymbol{\eta}_{\mathrm{ref}}$ and 1st-order Euler forward method, the nominal discrete model is obtained by omitting the estimation error $\dot{\boldsymbol{\xi}}$ as

$$\underbrace{\begin{bmatrix} \boldsymbol{e}(k+1) \\ \boldsymbol{e}_v(k+1) \end{bmatrix}}_{\boldsymbol{E}(k+1)} = \underbrace{\begin{bmatrix} \boldsymbol{I}_{3\times3} & \Delta t\boldsymbol{I}_{3\times3} \\ \boldsymbol{0}_{3\times3} & \boldsymbol{I}_{3\times3} \end{bmatrix}}_{\boldsymbol{A}_{\mathrm{mpc}}}\boldsymbol{E}(k) + \underbrace{\begin{bmatrix} \boldsymbol{0}_{3\times4} \\ \Delta t\boldsymbol{B}_F(k) \end{bmatrix}}_{\boldsymbol{B}_{\mathrm{mpc}}(k)}\boldsymbol{F}_{\mathrm{mpc}}(k), \tag{13}$$

where $\boldsymbol{e}_n$ is the nominal tracking error and $\boldsymbol{e}_{vn}$ is the nominal derivative of $\boldsymbol{e}_v = \dot{\boldsymbol{\eta}}_h - \dot{\boldsymbol{\eta}}_{\mathrm{ref}}$, Δt is the sampling time, $\boldsymbol{B}_F(k) = \boldsymbol{M}_\eta^{-1}(k)\boldsymbol{B}_\eta(k)$ is updated at each sampling but remains constant over the prediction horizon.

The MPC control objective is to make $\boldsymbol{E}(k)$ converge to zeros. To avoid undesirable tracking performance, the actual trajectory, orientation and velocities should be confined to the fol-

lowing constraints.

$$\mathbb{X}(k,\boldsymbol{\varepsilon}) = \left\{ \boldsymbol{E}(k) \left| \begin{array}{c} \sqrt{e_{n1}^2(k)+e_{n2}^2(k)} < \varepsilon_d \\ |e_{n3}| < \varepsilon_\psi \\ \sqrt{e_{vn1}^2(k)+e_{vn2}^2(k)} < \varepsilon_v \\ |e_{vn3}| < \varepsilon_r \end{array} \right. \right\}, \tag{14}$$

where e_{ni} and e_{vni} are the ith components of $\boldsymbol{e}_{ni}$ and $\boldsymbol{e}_{vni}$, respectively, $\boldsymbol{\varepsilon} = \left[\varepsilon_d, \varepsilon_\psi, \varepsilon_v, \varepsilon_r\right]$ are positive constants. Similar to (11), the boundaries for $\boldsymbol{F}_{\text{mpc}}$ are achieved using the constraints mapping defined below.

$$\boldsymbol{U}\left(\boldsymbol{F}_{h\min/\max}\right) = \boldsymbol{F}_{h\min/\max} - \boldsymbol{B}_\eta^+ \left[\boldsymbol{C}_\eta \dot{\boldsymbol{\eta}}_h + \boldsymbol{M}_\eta \left(\ddot{\boldsymbol{\eta}}_{\text{ref}} - \hat{\boldsymbol{D}}\right)\right].$$

The input constraint is therefore obtained as:

$$\mathbb{U}(k) = \left\{ \boldsymbol{F}_{\text{mpc}} \left| \boldsymbol{U}\left(\boldsymbol{F}_{h\min}\right) \le \boldsymbol{F}_{\text{mpc}} \le \boldsymbol{U}\left(\boldsymbol{F}_{h\max}\right) \right. \right\}. \tag{15}$$

To ensure the asymptotic stability under the finite prediction horizon, the error state in the Nth prediction should be forced to enter the terminal constraints $\mathbb{X}_f$ by a terminal law $\boldsymbol{u}_f$.

$$\mathbb{X}_f = \mathbb{X}(k+N, \boldsymbol{\varepsilon}_{\text{ter}}) \tag{16}$$

where $\boldsymbol{\varepsilon}_{\text{ter}} = \left[\varepsilon_{d\text{ter}}\ \varepsilon_{\psi\text{ter}}\ \varepsilon_{v\text{ter}}\ \varepsilon_{r\text{ter}}\right]$. The position and its terminal constraints can be interpreted as two round areas whose radius are deviation distances, as illustrated in Fig. 3.

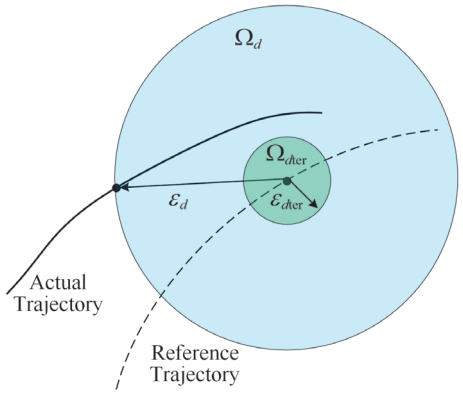

Figure 3. The schematic of the position constraints.

During the prediction interval $(N+1, +\infty)$, $\boldsymbol{u}_f$ aims to keep the tracking errors within $\mathbb{X}_f$ and ultimately converging to zeros. For this purpose, a sliding variable vector is defined by:

$$\boldsymbol{s}(k+N|k) = \boldsymbol{C}\boldsymbol{E}(k+N|k), \tag{17}$$

where $\boldsymbol{C} = [c_s \boldsymbol{I}_{3\times3}, \boldsymbol{I}_{3\times3}]$ is the weighting matrix, c_s should be selected to render the dynamics in sliding mode

$$\boldsymbol{e}_n(k+N+1|k) = (\boldsymbol{I}_{3\times3} - c_s\Delta t \boldsymbol{I}_{3\times3})\boldsymbol{e}_n(k+N|k) \tag{18}$$

asymptotically stable, which means $|1 - c_s\Delta t| < 1$. The terminal control is obtained by solving $\boldsymbol{s}(k+N+1|k) = \boldsymbol{0}$.

$$\boldsymbol{u}_f = \boldsymbol{K}_f \boldsymbol{E}(k+N|k), \tag{19}$$

where $\boldsymbol{K}_f = -\left(\boldsymbol{C}\boldsymbol{B}_{\text{mpc}}\right)^+ \boldsymbol{C}\boldsymbol{A}_{\text{mpc}}$ is the control gain matrix. Finally, the cost function with the following quadratic form is employed to penalize $\boldsymbol{E}(k+n|k)$, $\boldsymbol{E}(k+N|k)$ and $\boldsymbol{F}_{\text{mpc}}(k+n|k)$.

$$\begin{aligned} J_k = &\sum_{n=0}^{N-1} \left(\|\boldsymbol{E}(k+n|k)\|_{\boldsymbol{Q}}^2 + \left\|\boldsymbol{F}_{\text{mpc}}(k+n|k)\right\|_{\boldsymbol{R}}^2 \right) \\ &+ \|\boldsymbol{E}(k+N|k)\|_{\boldsymbol{P}}^2, \end{aligned} \tag{20}$$

where $\boldsymbol{Q} \in \mathbb{R}^{6\times6}$ and $\boldsymbol{R} \in \mathbb{R}^{4\times1}$ are positive definite weighting matrix, and $\boldsymbol{P} \in \mathbb{R}^{6\times6}$ is the solution of the discrete Lyapunov function.

$$\boldsymbol{P} = \left(\boldsymbol{A}_{\text{mpc}} + \boldsymbol{B}_{\text{mpc}}\boldsymbol{K}_f\right)^T \boldsymbol{P} \left(\boldsymbol{A}_{\text{mpc}} + \boldsymbol{B}_{\text{mpc}}\boldsymbol{K}_f\right) + \boldsymbol{Q} + \boldsymbol{K}_f^T \boldsymbol{R} \boldsymbol{K}_f$$

With the terminal cost function, Eq. (20) is monotonously decreasing, $J_{k+1}^* \le J_{k+1} \le J_k^*$, where J_k^* is the optimal solution of

the cost function at time instant k. This can be proven by

$$
\begin{aligned}
J_{k+1} &= \sum_{n=0}^{N-1}\left(\|\boldsymbol{E}(k+n+1\,|k+1)\|_{\boldsymbol{Q}}^2+\left\|\boldsymbol{F}_{\mathrm{mpc}}(k+n+1\,|k+1)\right\|_{\boldsymbol{R}}^2\right)\\
&+\|\boldsymbol{E}(k+N+1\,|k+1)\|_{\boldsymbol{P}}^2\\
&=\sum_{n=0}^{N-2}\left(\left\|\boldsymbol{E}(k+n+1\,|k)^*\right\|_{\boldsymbol{Q}}^2+\left\|\boldsymbol{u}(k+n+1\,|k)^*\right\|_{\boldsymbol{R}}^2\right)\\
&+\left\|\boldsymbol{E}(k+N\,|k)^*\right\|_{\boldsymbol{Q}}^2+\left\|\boldsymbol{K}_f\boldsymbol{E}(k+N\,|k)^*\right\|_{\boldsymbol{R}}^2\\
&+\left\|\left(\boldsymbol{A}_{\mathrm{mpc}}+\boldsymbol{B}_{\mathrm{mpc}}\boldsymbol{K}_f\right)\boldsymbol{E}(k+N\,|k)^*\right\|_{\boldsymbol{P}}^2\\
&=\sum_{n=0}^{N-2}\left(\left\|\boldsymbol{E}(k+n+1\,|k)^*\right\|_{\boldsymbol{Q}}^2+\left\|\boldsymbol{u}(k+n+1\,|k)^*\right\|_{\boldsymbol{R}}^2\right)\\
&+\left\|\boldsymbol{E}(k+N\,|k)^*\right\|^2_{\boldsymbol{Q}+\boldsymbol{K}_f^T R\boldsymbol{K}_f+\left(\boldsymbol{A}_{\mathrm{mpc}}+\boldsymbol{B}_{\mathrm{mpc}}\boldsymbol{K}_f\right)^T\boldsymbol{P}\left(\boldsymbol{A}_{\mathrm{mpc}}+\boldsymbol{B}_{\mathrm{mpc}}\boldsymbol{K}_f\right)}\\
&=\sum_{n=1}^{N-2}\left(\left\|\boldsymbol{E}(k+n\,|k)^*\right\|_{\boldsymbol{Q}}^2+\left\|\boldsymbol{u}(k+n\,|k)^*\right\|_{\boldsymbol{R}}^2\right)\\
&+\left\|\boldsymbol{E}(k+N\,|k)^*\right\|_{\boldsymbol{P}}^2\\
&=\sum_{n=0}^{N-2}\left(\left\|\boldsymbol{E}(k+n\,|k)^*\right\|_{\boldsymbol{Q}}^2+\left\|\boldsymbol{u}(k+n\,|k)^*\right\|_{\boldsymbol{R}}^2\right)-\left\|\boldsymbol{E}(k\,|k)^*\right\|_{\boldsymbol{Q}}^2\\
&-\left\|\boldsymbol{u}(k\,|k)^*\right\|_{\boldsymbol{R}}^2+\left\|\boldsymbol{E}(k+N\,|k)^*\right\|_{\boldsymbol{P}}^2\\
&=J_k^*-\left\|\boldsymbol{E}(k\,|k)^*\right\|_{\boldsymbol{Q}}^2-\left\|\boldsymbol{u}(k\,|k)^*\right\|_R^2
\end{aligned}
$$

which shows that the nominal system under the control is asymptotically stable.

Nominal MPC is employed to obtain the input $\boldsymbol{F}_{\mathrm{mpc}}$ by solving the following optimization problem. The nominal error state $\boldsymbol{E}(k)$ is updated by the perturbed actual tracking error at each sampling instant [20].

$$
\begin{aligned}
J_k^* &= \min_{\boldsymbol{F}_{\mathrm{mpc}}(k+n|k)} J_k\left(\boldsymbol{E}\left(k+n\,|k\right),\boldsymbol{F}_{\mathrm{mpc}}\left(k+n\,|k\right)\right)\\
s.t.&\begin{cases}
\boldsymbol{E}\left(k\,|k\right)=\boldsymbol{e}\left(k\right)=\boldsymbol{x}\left(k\right)-\boldsymbol{x}_{\mathrm{ref}}\left(k\right)\\
\boldsymbol{E}\left(k+1\,|k\right)=\boldsymbol{A}_{\mathrm{mpc}}\boldsymbol{E}\left(k\right)+\boldsymbol{B}_{\mathrm{mpc}}\left(k\right)\boldsymbol{F}_{\mathrm{mpc}}\left(k\right)\\
\boldsymbol{F}_{\mathrm{mpc}}\left(k+n\,|k\right)\in\mathbb{U}\\
\boldsymbol{E}\left(k+n\,|k\right)\in\mathbb{X}\\
\boldsymbol{E}\left(k+N\,|k\right)\in\mathbb{X}_f,
\end{cases}
\end{aligned}
\tag{21}
$$

where $\boldsymbol{x}=\left[\boldsymbol{\eta}_h\;\dot{\boldsymbol{\eta}}_h\right]^T$ is the actual state and $\boldsymbol{x}_{\mathrm{ref}}$ is the reference. By [20], we obtain the following results.

Theorem 2. *For the system (12) in the presence of the estimation error $\dot{\boldsymbol{\xi}}$, the control of $\boldsymbol{F}_{\mathrm{mpc}}$ and the observation law (8) are able to steer the terminal nominal tracking error based on any sampling instant into the terminal constraint, namely, $\boldsymbol{E}\left(k+N\,|k\right)\in\mathbb{X}_f,\forall k\in\mathbb{Z}^+$.*

SIMULATION RESULTS

We conduct a simulation study to validate the control design for a horizontal trajectory tracking scenario in the presence of unknown currents and hydrodynamics. In simulation, a 1st-order Gauss-Markov process is used to generate the unknown average current velocity [17]. Therefore, the instant magnitude of current velocity $V_c\left(t\right)$ can be defined as

$$
\dot{V}_c\left(t\right)=\begin{cases}\omega\left(t\right) & V_{\min}\le V_c\left(t\right)\le V_{\max}\\ -\omega\left(t\right) & \text{otherwise,}\end{cases}
\tag{22}
$$

where $\omega\left(t\right)$ is a Gaussian white noise, $V_{\min}$ and $V_{\max}$ are boundaries for current velocity. The initial current velocity should be $V_c\left(0\right)=\frac{1}{2}\left(V_{\min}+V_{\max}\right)$.

The irrotational current velocity vector in $\{b\}$ can be defined in terms of sideslip angle β and yaw angle ψ.

$$
\boldsymbol{v}_{hc}^b=\begin{bmatrix}V_c\cos\left(\beta-\psi\right)\\ V_c\sin\left(\beta-\psi\right)\\ 0\end{bmatrix}
\tag{23}
$$

Due to the symmetry, the horizontal hydrodynamics is modeled using the following equations.

$$
\boldsymbol{M}_A=-\mathrm{diag}\left(X_{\dot{u}},Y_{\dot{v}},N_{\dot{r}}\right),\;\boldsymbol{C}_{hA}\left(\boldsymbol{v}\right)=\begin{bmatrix}0 & 0 & Y_{\dot{v}}v\\ 0 & 0 & -X_{\dot{u}}u\\ -Y_{\dot{v}}v & X_{\dot{u}}u & 0\end{bmatrix}
$$

and $\boldsymbol{D}_h=-\mathrm{diag}\left(X_u,Y_v,N_r\right)$, where $\boldsymbol{M}_A$, $\boldsymbol{C}_{hA}$ and $\boldsymbol{D}_h$ are added mass matrix, hydrodynamic Coriolis and centripetal matrix, and hydrodynamic damping matrix, respectively, $X_{\dot{u}}$, $Y_{\dot{v}}$, $N_{\dot{r}}$, X_u, Y_v and N_r denote the hydrodynamics coefficients.

The BlueROV is expected to track a circle on the surface. The desired position and orientation in $\{i\}$ are defined correspondingly as follows.

$$
\boldsymbol{\eta}_{\mathrm{ref}}=\begin{bmatrix}R_{\mathrm{ref}}\cos\varphi\\ R_{\mathrm{ref}}\left(1+\sin\varphi\right)\\ \pi/2+\varphi\end{bmatrix}
\tag{24}
$$

and $\varphi=\varphi_0+r_{\mathrm{ref}}t$, where R_{ref} is the reference radius, φ is the rotational angle with respect to the positive direction of x axis, φ_0 is the initial angle, r_{ref} denotes the desired angular velocity, and t represents time.

The inertial parameters used in this simulation are defined as $m=10$ kg, $I_z=2$ kgm^2, and $\boldsymbol{r}_{hg}=\left[x_g\;y_g\right]^T=\left[0.01\;0.01\right]^T$m, which is the offset vector between C_g and C_m. The hydrodynamic coefficients are defined proportionally according to the

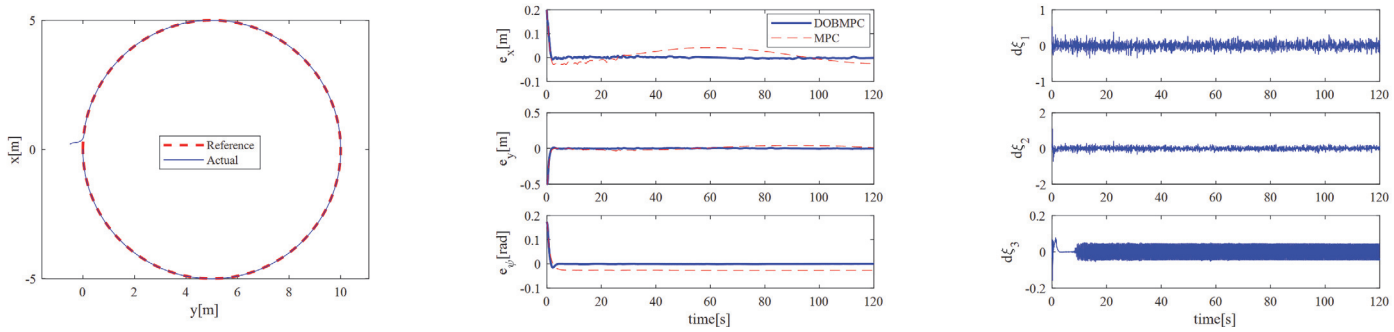

Figure 4. (a) Horizontal position. (b) Tracking errors. (c) Estimation errors.

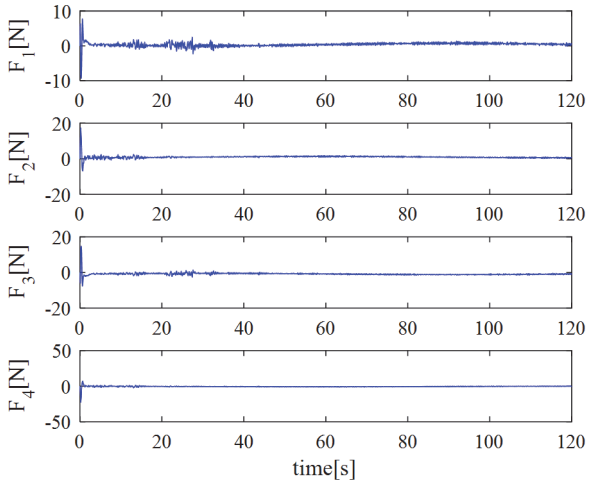

Figure 5. The controlled thrusts.

Table 1. The used values of the DOBMPC parameters.

Para.	Value	Para.	Value
$\boldsymbol{Q}$	$\mathrm{diag}\,(20,25,10$ $20,25,10)$	$\boldsymbol{\varepsilon}_{\mathrm{ter}}$	$\left[0.01,\frac{\pi}{180},0.01,\frac{\pi}{180}\right]$
$\boldsymbol{R}$	$\mathrm{diag}\,(2,2,2,2)$	$\boldsymbol{K}_1$	$\mathrm{diag}\,(10,10,8)$
c_s	$\frac{1.01}{\Delta t}$	$\boldsymbol{K}_2$	$\mathrm{diag}\,(0.03,0.02,0.011)$
$\boldsymbol{\varepsilon}$	$\left[0.5,\frac{\pi}{18},0.5,\frac{\pi}{18}\right]$		

scale of BlueROV2 compared with the robot used in [7], $X_u = -7.2$ kgs^{-1}, $Y_v = -7.7$ kgs^{-1}, $N_r = -3$ kgms^{-1}, $X_{\dot{u}} = -2.9$ kg, $Y_{\dot{v}} = -3$ kg and $N_{\dot{r}} = -3.3$ kgm. Reference parameters are selected as $R_{\mathrm{ref}} = 5$ m, $r_{\mathrm{ref}} = \frac{\pi}{60}$ rads^{-1} and $\varphi_0 = -\frac{\pi}{2}$ rad. Configuration parameters are set as $L_h = 0.145$ m, $W_h = 0.1$ m, $\gamma_1 = -\frac{\pi}{4}$, $\gamma_2 = \frac{\pi}{4}$, $\gamma_3 = \frac{3\pi}{4}$ and $\gamma_4 = -\frac{3\pi}{4}$. The covariance of Gaussian noise is 0.01, and the boundaries of current velocity are defined as $V_{\min} = 0$ ms^{-1} and $V_{\max} = 0.1$ ms^{-1}. The thruster constraints are $F_{\min} = -40$ N and $F_{\max} = 50$ N. The initial states are set as $\boldsymbol{\eta}_h(0) = \left[0.2\,\mathrm{m}, -0.5\,\mathrm{m}, \frac{\pi}{18}\,\mathrm{rad}\right]^T$ and $\boldsymbol{v}_h^b = \left[0\,ms^{-1}, 0\,ms^{-1}, 0\,rads^{-1}\right]^T$. The controller parameters are shown in Table 1. The optimization problem (21) is solved online by a Sequence Quadratic Program (SQP) with $\Delta t = 0.1$s and $N = 10$.

The values of the sample time and prediction horizon are chosen under the consideration of real application and computational complexity. The excellent tracking performance is illustrated in Fig.**??**. Given the initial deviation, the actual trajectory reaches the reference quickly and keep on it accurately. Further decreasing sample time or increasing prediction horizon cannot improve the performance significantly. The performance can be further demonstrated by comparing with the traditional MPC, as shown in Fig. 4(b). Without the disturbance observer, the tracking errors oscillate around zeros in the x and y directions, and there is a steady error in yaw direction. However, under the control of DOBMPC, all errors decay quickly and converge to zeros in an asymptotical stable manner, which suggests the good robustness to the unknown disturbances.

The estimation errors, as shown in Fig. 4(c), are stable in the sense of Lyapunov. The reason why they do not present asymptotical stability may be that the coupling between the disturbances is not taken into account in the observer gain matrix. Fig. 5 shows that the four thrusts vary dramatically in order to cancel the initial deviation and then become stable around zeros to keep the AUV moving along with the reference.

CONCLUSION AND FUTURE WORK

In this paper, a disturbance observer based model predictive control (DOBMPC) was presented for small AUV trajectory tracking. The control system design consists of the MPC de-

sign with an integration of the feedback linearization law to be applied to the perturbed AUV system. The disturbances were estimated by a STA-based observer and then used in the control design. The simulation results using BlueROV2 as an example show the superior tracking performance of the proposed method. The comparison with the traditional MPC control was also included in the paper.

In the future, the work can be expanded by considering the following aspects: (1) Localization: not all feedback signals are measurable and the states estimator is required and the navigation error should be taken into account in controller design. (2) System identification: system inertial parameters, such as inertia tensor matrix and offset distance, may not be obtained accurately or known in prior. For this reason, adaptive controller or identification algorithm would be employed.

ACKNOWLEDGMENT

The authors would like to thank Mehdi Rahmati and Seth Karten of Rutgers University for their help working with the AUV. This work was partially supported by US National Science Foundation under award CNS-1739315.

REFERENCES

[1] Wang, P., Singh, P. K., and Yi, J., 2013. "Dynamic model-aided localization of underwater autonomous gliders". In Proc. IEEE Int. Conf. Robot. Autom., pp. 5545–5550.

[2] Soylu, S., Proctor, A. A., Podhorodeski, R. P., Bradley, C., and Buckham, B. J., 2016. "Precise trajectory control for an inspection class ROV". pp. 508–523.

[3] Gomes, R. M. F., Sousa, J. B., and Pereira, F. L., 2003. "Modeling and control of the IES project ROV". In Proc. Europ. Control Conf., pp. 3424–3429.

[4] Dyda, A. A., Oskin, D., and S. Longhi, A. M., 2016. "A nonlinear system with coupled switching surfaces for remotely operated vehicle control". In 10th IFAC Conf.Control Appl. Marine Syst., pp. 311–316.

[5] Zhang, M. J., and Chu, Z. Z., 2012. "Adaptive sliding mode control based on local recurrent neural networks for underwater robot". pp. 56–62.

[6] Bessa, W. M., Dutra, M. S., and Kreuzer, E., 2008. "Depth control of remotely operated underwater vehicles using an adaptive fuzzy sliding mode controller". *Robot. Auton. Syst.,* ***56***, pp. 670–677.

[7] Soylu, S., Buckham, B. J., and Podhorodeski, R. P., 2008. "A chattering-free sliding-mode controller for underwater vehicles with fault-tolerant infinity-norm thrust allocation". pp. 1647–1659.

[8] Sebastian, E., and Sotelo, M. A., 2007. "Adaptive fuzzy sliding mode controller for the kinematic variables of an underwater vehicle". *J. Intelli. Robot. Syst.,* ***49***, pp. 189–215.

[9] Bessa, W. M., Dutra, M. S., and Kreuzer, E., 2010. "An adaptive fuzzy sliding mode controller for remotely operated underwater vehicles". *Robot. Auton. Syst.,* ***58***, pp. 16–26.

[10] Valdovinos, L. G. G., Jimenez, T. S., and Rodriguez, H. T., 2009. "Model-free high order sliding mode control for ROV: Station-keeping approach". In IEEE OCEANS, pp. 1–7.

[11] Barahona, R. R., Vega, V. P., Diaz, E. O., and Ubando, L. M., 2011. "A model-free backstepping with integral sliding mode control for underactuated ROVs". In IEEE Int. Conf. Electr. Eng. Comp. Sci. Automat. Contr., pp. 1–7.

[12] Valdovinos, L. G. G., Jimenez, T. S., Sanchez, M. B., Balanzar, L. N., Alvarado, R. H., and Ledesma, J. A. C., 2014. "Modeling, design and robust control of a remotely operated underwater vehicle". *Int. J. Adv. Robotics Syst.,* ***11***(1), pp. 1–16.

[13] Molero, A., Dunia, R., Cappelletto, J., and Fernandez, G., 2011. "Model predictive control of remotely operated underwater vehicle". In Proc. IEEE Conf. Decision Control, pp. 2058–2063.

[14] Shen, C., Shi, Y., and Buckham, B., 2016. "Nonlinear model predictive control for trajectory tracking of an AUV: A distributed implementation". In Proc. IEEE Conf. Decision Control, pp. 5998–6003.

[15] Abraham, I., and Yi, J., 2015. "Model predictive control of buoyancy-driven autonomous underwater gliders". In Proc. Amer. Control Conf.

[16] Fossen, T. I., 2011. *Handbook of Marine Craft Hydrodynamics and Motion Control*. John Wiley and Sons Inc, Noida, India.

[17] Fossen, T. I., 1994. *Guidance and Control of Ocean Vehicles*. John Wiley and Sons Inc.

[18] Wang, B. H., Meng, Z. J., and Huang, P. F., 2017. "Attitude control of towed space debris using only tether". *Acta Astronautica,* ***138***, pp. 152–167.

[19] Guermouche, M., Ali, S. A., and Langlois, N., 2015. "Super-twisting algorithm for DC motor position control via disturbance observer". In 9th IFAC Symp. Control Power Energy Syst., pp. 43–48.

[20] Sun, Z. Q., Dai, L., Liu, K., Xia, Y., and Johansson, K. H., 2018. "Robust MPC for tracking of nonholonomic robots with additive disturbances". *Automatica*. in press.